Published in final edited form as:
Nanomedicine. 2011 April ; 7(2): 123–130. doi:10.1016/j.nano.2010.09.004.

Endocytosis of Titanium Dioxide Nanoparticles in Prostate Cancer PC-3M Cells

Kenneth T. Thurn, PhD,
Department of Radiation Oncology, Northwestern University Feinberg School of Medicine Chicago, IL 60611

Hans Arora,
Department of Radiation Oncology, Northwestern University Feinberg School of Medicine Chicago, IL 60611

Tatjana Paunesku, PhD,
Department of Radiation Oncology, Northwestern University Feinberg School of Medicine Chicago, IL 60611

Aiguo Wu, PhD,
Division of Functional Materials and Nanodevices, Ningbo Institute of Material Technology and Engineering, Chinese Academy of Sciences, No. 519 Zhuangshi Rd. Zhenhai District, Ningbo City, Zheijang Province, 315201 P.R. China

Eric M.B. Brown, PhD,
Department of Biological Sciences, University of Wisconsin-Whitewater, Upham Hall, Room 357, 800 W. Main St., Whitewater Wisconsin 53190-1790

Caroline Doty,
Department of Radiation Oncology, Northwestern University Feinberg School of Medicine Chicago, IL 60611

Jeff Kremer, and
Department of Radiation Oncology, Northwestern University Feinberg School of Medicine Chicago, IL 60611

Gayle Woloschak, PhD*
Department of Radiation Oncology, Department of Radiology, and Department of Cell and Molecular Biology, Northwestern University Feinberg School of Medicine Chicago, IL 60611

Kenneth T. Thurn: k-thurn@northwestern.edu; Hans Arora: h-arora@northwestern.edu; Tatjana Paunesku: tpaunesku@northwestern.edu; Aiguo Wu: auguo@nimte.ac.cn; Eric M.B. Brown: browne@uww.edu; Caroline Doty: caroline-doty@northwestern.edu; Jeff Kremer: jeffckremer@gmail.com; Gayle Woloschak: g-woloschak@northwestern.edu

Abstract

Nanotechnology has introduced many exciting new tools for the treatment of human diseases. One of the obstacles in its application to that end is the lack of a fundamental understanding of the interaction that occurs between nanoparticles and living cells. This report describes the

* Corresponding Author: Professor Gayle Woloschak, 303 E. Chicago Ave., Ward Building Room 13-007, Chicago IL, 60611 (USA), g-woloschak@northwestern.edu.

quantitative analysis of the kinetics and endocytic pathways involved in the uptake of anatase titanium dioxide (TiO_2) nanoparticles into prostate cancer PC-3M cells. The experiments were performed with TiO_2 nanoconjugates—6 nm nanoparticles with surface conjugated fluorescent Alizarin Red S (ARS). Results obtained by flow cytometry, fluorescence microscopy, and inductively-coupled plasma mass spectrometry confirmed a complex nanoparticle-cell interaction involving a variety of endocytic mechanisms. The results demonstrated that a temperature, concentration, and time-dependent internalization of the TiO_2 nanoparticles and nanoconjugates occurred via clathrin-mediated endocytosis, caveolin-mediated endocytosis, and macropinocytosis.

Keywords

anatase; TiO_2; nanoconjugate; endocytosis; Alizarin Red S

Introduction

The photo-catalytic properties of titanium dioxide (TiO_2) have led to extensive research into its potential uses as a disinfectant, antibiotic, biological sensor, tumor cell killing agent, and a gene targeting device [1-9]. Bulk forms of TiO_2 are generally biologically and chemically inert [3, 10-14], however, surface of of TiO_2 nanoparticles smaller than 20 nm is reactive due to surface defects and readily binds enediol bidentate ligands including dopamine, ascorbic acid, alizarin, and Alizarin Red S (ARS) [15-17]. Herein, we take advantage of earlier work by our group demonstrating a stable covalent bond between TiO_2 nanoparticles smaller than 20nm and fluorescent ARS molecules[15]. In this work, TiO_2-ARS nanoconjugates have been shown to be resistant to intracellular milieu for more than 12h well beyond the timepoints used in experiments described here[15]. Therefore, conjugation of ARS permits us to “dissect” nanoconjugate uptake in living cells using confocal microscopy and flow cytometry.

There are three main types of endocytosis in non-phagocytic cells. They are: Clathrin Mediated Endocytosis (CME), Caveolin-Mediated Endocytosis (Cav-Me), and Macropinocytosis. There also exist minor forms of endocytosis (e.g. dynamin dependent clathrin independent and dynamin and clathrin independent endocytosis) which have not yet been fully elucidated [18-20]. Endocytic pathways can be inhibited with various pharmacological agents, dominant negative proteins, and cellular treatments. Clathrin coated vesicles can be reduced nearly 80% by potassium depletion [21]. CME and Cav-Me can be inhibited by dominant negative forms of dynamin I (K44A) since this protein is involved in the budding off of vesicles in both types of endocytosis [22]. Cav-Me can also be inhibited by treatment with micromolar concentrations of the tyrosine kinase inhibitor, genistein [23]. Macropinocytosis is an actin dependent mechanism, and treatment with actin polymerization inhibitor cytochalasin D is often used to repress this process. Since actin is involved in most major endocytic processes, [24-25] treatment with the amiloride derivative, 5-(N-ethyl-N-isopropyl) amiloride (EIPA) is considered to be a more specific macropinocytosis inhibitor. Amiloride and EIPA are Na^+/H^+ exchange inhibitors that reduce macropinocytosis at mM or μM concentrations, respectively [26].

The endocytosis of nanoparticles depends on the size, shape, and charge of the nanoparticles, and also on the cell type treated [22, 27-30] (reviewed in [31]). Although TiO_2 has been studied for nearly three decades, the endocytic pathways involved in its uptake have yet to be fully discerned, possibly because there are so many different forms of this oxide, and such a variation in particle shapes and sizes; e.g. “ultrafine” TiO2 was found in clathrin-coated vesicles of lung epithelial cells by electron microscopy [32] Our group focuses on work with nanoparticles smaller than 20nm, especially those that are directly labeled with fluorescent ARS[15]. Previous work established that: (i) TiO2-ARS nanoconjugates emit

detectable fluorescence that can be analyzed by both confocal fluorescent microscopy and flow cytometry; (ii) a sample preparation procedure that removes surface adsorbed nanoconjugates was established, allowing both single cell and cell population analyses; (iii) nanoconjugates were stable in cultured animal cells, including the PC3-M cells; and (iv) the minimal number on nanoconjugates to obtain a confocal fluorescent signal is about 10^4 [15]. Herein, we expanded upon those results to utilize fluorescence microscopy and flow cytometry in order to characterize the uptake of TiO_2-ARS nanoconjugates in PC-3M cells. This uptake is temperature, time, and concentration dependent; while competition experiments with excess unlabeled nanoparticles revealed dependence on available membrane binding sites. All three of the major endocytosic pathways were involved in the nanoconjugate uptake: clathrin-mediated endocytosis, caveolin-mediated endocytosis, and macropinocytosis. These experiments were repeated with the unlabeled nanoparticles quantified by Inductively Coupled Plasma Mass Spectroscopy (ICP-MS) to verify that the results were not dependent upon the ARS conjugation.

Materials and Methods

Nanoparticle Synthesis and Nanoconjugate Preparation

Nanoconjugates were prepared from the same batch of nanoparticles that were synthesized, characterized and used in our earlier work[15, 33] employing the same approach that was described therein. In short, TiO_2 nanoparticles with average diameter of 6 nm (nanoparticle dispersity 21%) were synthesized by low-temperature alkaline hydrolysis route as described previously [1], and were dialyzed and stored at 4°C in 10 mM Na_2HPO_4 buffer pH = 6.5. The molarity of nanoparticles was 10 μM, hence their surface was calculated at 6.9 mM potential binding sites. Conjugation of alizarin red s (ARS) to the nanoparticle surface was done prior to each experiment as described previously [15], by incubating bare nanoparticles with ARS in appropriate molar ratio to cover 44% of the nanoparticles surface binding sites with ARS. E.g. 1 ml of 10 μM nanoparticles was mixed with 0.864 ml of 8 mM Alizarin Red S; resultant solution was 0.563 μM with respect to nanoparticles. Subsequently, nanoparticle solution was further diluted to concentrations indicated in each specific case. UV-visible light spectroscopy (using Nanodrop ND-1000 Spectrophotometer; NanoDrop Technologies Inc.) for absorbances between 200-750 nm showed characteristic red shift in absorption peak identified previously as unique to the nanoconjugates.[15]

Cell Culture Conditions

All cell culture reagents were purchased from Mediatech Inc. (Manassas VA) unless otherwise specified. PC-3M metastatic prostate cancer cells with stable GFP expression were a gift from Dr. Raymond Bergan, Northwestern University [34]; these cells were used in our prior work establishing intracellular stability of nanoconjugates[15]. PC-3M cells were maintained at 37°C with 5% CO_2 in RPMI 1640 media supplemented with 10% fetal bovine serum (FBS), 2 mM L-glutamine, 10 mM HEPES, 100 I.U./ml penicillin, 100 μg/ml streptomycin, and 0.15 mg/ml of G418 sulfate. Prior to cell treatments, the cells were washed with phosphate buffered saline solution (PBS) and placed in serum free RPMI 1640 medium for 1-2 hours. Next, the cells were treated with TiO_2-ARS nanoparticles (0-200nM), TiO_2 nanoparticles (0-540nM), or Alizarin Red S alone (0-60 μM). After treatment cells were washed with PBS, then in 200 mM glycine pH 4 (Sigma Aldrich, St. Louis MO) and two more times in PBS. Only exception was the experiment described in Figure 1B where only PBS washes were done.

Inhibition of Endocytosis

For the temperature-dependant effects on uptake, cells were pre-incubated for one hour at either 4°C or 37°C prior to treatment with nanoparticles at the same temperatures. For

potassium depletion, cells were washed in an isotonic potassium-free medium (140 mM NaCl, 1 mM $CaCl_2$, 1mM MgCl, 5.5 mM d-Glucose, 20 mM HEPES), then placed in a hypotonic solution (v:v potassium free-medium: water) for 10 minutes. Next, the cells were washed and incubated for 30 minutes in the isotonic potassium-free medium. Finally, cells were treated with nanoconjugates or a positive control marker 50 μg/ml of Transferrin-Alexa Fluor 633 (Invitrogen). As a control, cells were treated with the same solutions supplemented with 20 μM KCl. Endocytosis inhibitors 5-(N-Ethyl-N-isopropyl) amiloride (EIPA) and genistein were incubated with cells for one hour prior to treatment with markers or nanoparticles. For macropinocytosis inhibition, cells were treated with 60 μM of EIPA prior to nanoconjugate or dextran treatment. To inhibit caveolin-mediated endocytosis, cells were treated with 100 μM of genistein before nanoconjugate or BODIPY-LacCer treatment.BODIPY-LacCer was added to cells at 4°C and incubated for 30 minutes. Then the cells were placed at 37°C to allow endocytosis. After one hour, cells were washed 4 times for 10 minutes in RPMI 1640 supplemented with 5% defatted bovine serum albumin (Sigma-Aldrich); 2 μM BODIPY FL C_5-lactosylceramide (LacCer) (Invitrogen) as a positive control for caveolin-mediated endocytosis. In experiments with EIPA, marker for macropinocytosis was 250 μg/ml of Dextran-Alexa Fluor647 (10,000 MW, Invitrogen).

Flow Cytometry and Cell Sorting

PC-3M cells for flow cytometry were grown until approximately 30-40% confluent. After treatment and washing, cells were trypsinized, collected in FBS supplemented medium, and brought to a single cell suspension. Samples were analyzed or sorted at the Northwestern University Flow Cytometry Core Facility of the Robert H. Lurie Cancer Center on the DakoCytomation MoFlo Flow Cytometer (Dako, Denmark). TiO_2-ARS nanoconjugates were excited by a 543 nm laser. Positive controls for CME, macropinocytosis and Cav-Me: Alexa Fluor transferrin 633; Dextran-Alexa Fluor 647 and BODIPY-LacCer were excited by a 630 nm laser. In all cases, fluorescence was quantified by the number of cells that emitted above the level of autofluorescence in control cells. Analysis was performed using the FCS Express V3 program (De Novo Software, Los Angeles CA). Cell debris was excluded based on the forward and side scatter characteristics of the cell populations.

Confocal Microscopy

For confocal microscopy cells were cultured on glass coverslips. After treatment and washes the cells were fixed in 4% paraformaldehyde, stained with Hoechst 33343 (Invitrogen), and mounted onto slides in mounting medium (9 mM p-phenylenediamine, 10 mM Tris pH 8, 70% glycerol). Samples were visualized using the LSM 510 UV Meta Microscope (Carl Zeiss, Inc., Maple Grove, MN) at the Northwestern University Cell Imaging Facility. Lasers of 405 nm, 488 nm, and 543 nm were used with bandpass filters of 420-480 nm, 505-530 nm, 560-615 nm, respectively.

Inductively Coupled Plasma Mass Spectroscopy (ICP-MS)

Cells were treated as described above, with uncoated TiO_2 nanoparticles. After washing, cells were collected by scraping, centrifuged at 5,000 g for 5 minutes, and washed in 3% HNO_3. The samples were then incubated at 65°C in HNO_3 overnight. Several dilutions were done to bring the titanium atoms to within a 0-50 parts per billion range (ppb), for which we prepared titanium standard curve. All samples and standards included internal standards of 3 ppb of Indium. Samples were run with the SC-2 Autosampler (Elemental Scientific Inc., Omaha NE) and analyzed by the X-Series II ICP-MS (Thermo Scientific, Waltham MA) at the Northwestern University, Quantitative Bioelemental Imaging Center.

Statistical Analysis

Data were analyzed using the GraphPad InStat 3 software (GraphPad Software Inc., La Jolla CA). Unpaired two-tail P value t tests were performed to compare the percentages of fluorescent cells, or the mean fluorescence intensities (arbitrary units) of the cell populations ($n \geq 3$). P values less than 0.05 were considered significant.

Experimental Results

Prostate cancer cells PC-3M were treated with 0-200 nM (0-16 ng/ml) of 6 nm TiO_2-ARS nanoconjugates for one hour, alone or in the presence of "competitor" non-labeled TiO_2 nanoparticles. About 44% of the nanoparticle surface titanium atoms were conjugated to ARS molecules, using the procedure described previously [15]. Coating of the nanoparticles with ARS permitted fluorescent detection of nanoconjugates, while treatment with ARS alone did not result in appreciable intracellular fluorescence as shown before [15]. In order to decrease false positive results from nanoconjugates passively adhering to the cellular plasma membrane, here and wherever it is not emphasized otherwise the cells were washed with 200 mM acidic glycine (pH=4) at the conclusion of each treatment.

Results in Figure 1A demonstrated a concentration-dependent increase in fluorescence in cells treated with an increased concentration of nanoconjugates. Approximately 13% of the cell population treated with 10 nM of TiO_2-ARS nanoconjugates emitted detectable fluorescence after one hour of treatment, compared to over 50% of the cells treated with 50 nM nanoconjugates (equal to 4 ng/ml of TiO_2 in media). The nanoconjugate uptake reached saturation level at about 100 nM under the conditions used (1 hour treatment). In subsequent experiments concentration of 50 nM TiO_2-ARS was used.

In Figure 1B cells were treated with 50 nM TiO_2-ARS nanoconjugates either alone or in the presence of 135 fold excess of unlabeled TiO_2 nanoparticles. This concentration of unlabeled nanoparticles was selected as non-toxic, experimentally feasible and likely to completely outcompete fluorescent nanoconjugates when monitored by confocal microscopy. Moreover, we anticipated that even passive adherence of nanoconjugates to the cell surface would be prevented in this case and for that reason in this experiment alone we did not perform the glycine wash of the cells prior to microscopy in order to preserve passive competitor nanoparticle interactions. PC-3M cells stably expressing green fluorescent protein (GFP) (green) treated with TiO_2-ARS nanoconjugates alone, exhibited a strong ARS signal (maroon) both within the cell, in large cytoplasmic vesicles, and on the cell surface. When these cells were treated simultaneously with the nanoconjugates and non-fluorescent nanoparticles, showed no detectable fluorescence on the cell surface or within the cytoplasm. The morphology of the cell was also altered at this treatment concentration (540 ng/ml of TiO_2), with large vacuoles void of GFP within the cell, possibly filled with nanoparticles.

The effect of incubation time (0-120 minutes) on uptake was also investigated (Figure 2). TiO_2-ARS fluorescence was analyzed by flow cytometry to quantify uptake as a percentage of the cell population that had internalized the nanoconjugates. Figure 2A shows that after 5 minutes of treatment, approximately 8% of cells exhibited fluorescence, after 15 minutes 25%, and at one-hour nearly 50% of the cells. These results were verified with confocal microscopy (Figure 2B). TiO_2-ARS nanoconjugate aggregates were visible both on the cell surface and within the cells at 5 minutes of treatment, while at 60 minutes large aggregates were found in perinuclear regions and throughout the cytoplasm.

To investigate the effect of cellular metabolism on the uptake of TiO_2-ARS nanoconjugates, cells were incubated at 4°C prior to, and during the treatment with nanoconjugates (Figure

3). PC-3M cells were treated with 50 nM of TiO_2-ARS for one hour at either 4°C or 37°C, and the fluorescence from TiO_2-ARS was quantified by flow cytometry. Uptake at 37°C was robust and similar to previous experiments (58%), but severely diminished in cells treated at 4°C (10%) (Figure 3). When comparing untreated control cells (false positive fluorescence at 1%) with cells treated at 4°C (10%) there was a statistically significant increase in cellular ARS (nanoconjugate) associated fluorescence. This suggested that both metabolically dependent uptake and metabolically-independent adhesion of nanoconjugates to the cell surface occurred at the same time.

To evaluate the contribution of each of the three main energy dependent pathways of non-phagocytic endocytosis on the internalization of TiO_2-ARS nanoconjugates, each mechanism was inhibited in turn (Figure 4). Prior to nanoconjugate treatment, CME was abolished by depletion of cellular potassium [35-36]. Depleting cellular levels of potassium prevented interaction between clathrin and adapter proteins at the cell membrane which stabilize clathrin-coated pits [37]. Fluorescently labeled transferrin (Alexa Fluor 633) was used as a positive control for CME [18]. After treatment, extracellular transferrin was removed from the cell surface by treatment with pronase. Figure 4A shows that cells devoid of potassium (-KCl) exhibited a statistically significant decrease in the number of cells that internalized transferrin and a significant reduction in cells displaying TiO_2-ARS associated fluorescence (54% and 53%, respectively).

In Figure 4B, 5-(N-Ethyl-N-isopropyl) amiloride (EIPA) was used to inhibit macropinocytosis. Cells were pre-treated with 60 μM EIPA before incubation with fluorescently labeled dextran-Alexa647, used as a marker of macropinocytosis. The uptake of dextran was inhibited by EIPA by 40% ($p<0.05$), while the reduction in the nanoconjugate uptake reached 54%.

Cav-Me (Figure 4C) was inhibited by treatment of cells with 100 μM of genistein; BODIPY-LacCer, a fluorescent sphingolipid analog that was used as a positive control [38]. Due to the partial overlap between fluorescent emission spectra of BODIPY-LacCer and GFP, cells were analyzed not as a percentage of cells that had internalized the sphingolipid, but instead based on the cell population's mean fluorescence intensity. Untreated cells and cells treated with BODIPY-LacCer at 4°C were used as negative controls to determine the baseline fluorescence intensity. Cells pretreated with genistein showed a statistically significant 34% decrease in BODIPY associated fluorescence. Genistein treatment also caused a decrease in TiO_2-ARS fluorescence, although only marginally statistically significant ($0.1>p>0.05$).

All of the flow cytometry experiments were performed with TiO_2-ARS nanoconjugates, therefore, to verify that this surface modification did not affect the cellular uptake pathways, total titanium content was directly quantified in cells treated with uncoated nanoparticles. Inductively Coupled Plasma Mass Spectrometry (ICP-MS) was used for these experiments. Cells were treated with the same concentration of nanoparticles (50 nM), with or without inhibition of endocytic pathways. Inhibition was performed in the potassium-free medium supplemented or not with KCl to regulate CME (Figure 5A), or in the presence of serum free RPMI 1640 medium with or without the pharmacological agents targeting macropinocytosis or Cav-Me (Figure 5B). After treatment, cells were extensively washed, collected and resuspended in 3% nitric acid (HNO_3) and incubated overnight at 65°C. Finally, samples were analyzed by ICP-MS to determine the level of titanium isotopes 47-49. Titanium 48 is the most prevalent form of titanium and was used for analysis.

Cells treated at 4°C displayed a statistically significant decrease in cell associated titanium 48 compared to cells treated at physiological temperatures in either potassium-free medium

supplemented with KCl (52% reduction, Figure 5A, $p<0.05$), or in RPMI 1640 medium (60% reduction, Figure 5B, $p<0.05$). This confirmed the dependence of TiO_2 nanoparticle endocytosis on active metabolism.

The concentration of titanium was also reduced in each of the three conditions that inhibit endocytic pathways. In cells depleted of KCl, titanium was reduced by 28% compared to KCl supplemented cells (Figure 5A). In samples where macropinocytosis was inhibited by pre-incubation with EIPA (Figure 5B), titanium 48 was decreased by 32% compared to control cells. In the presence of genistein, cellular associated titanium 48 was decreased by 28% compared to control cells. These trends determined by ICP-MS in cells treated with uncoated nanoparticles were similar to those observed by flow cytometry where the extent of ARS fluorescence represented nanoconjugate uptake (Figures 3 and 4).

Discussion

Despite the great variety of different nanoparticle forms of TiO_2 and the widespread actual and potential use of TiO_2, relatively few studies focused on the cellular uptake of TiO_2 nanoparticles and nanoconjugates as reviewed recently by Suh and Suslick.[39] It is very likely that this omission is a result of inherent difficulties with identification of TiO2 by light microscopy. Unlike gold nanoparticles or carbon nanotubes that can be uniquely monitored by Plasmon resonance or Raman spectroscopy, TiO_2 is not associated with any unique detection technique, is non-fluorescent and has a low density which makes it inconvenient for other than X-ray fluorescence detection. However, its surface defects allow for a stable covalent surface modification with bidentate ligands—one of them is a fluorescent dye ARS[15]. Herein, we used TiO_2-ARS nanoconjugates to investigate endocytosis of TiO_2 nanoparticles.

The form of endocytosis involved in nanoparticle uptake can be expected to affect the nanoparticle's intracellular localization and trafficking. Understanding endocytosic mechanisms is vital for the development of nanomaterials for clinical therapies. The frequent alterations in the endocytic pathways of various malignant cells make these studies especially significant, as targeting of specific pathways becomes feasible with rationally modified nanoparticles [20, 40]. In three closely related prostate cancer cell lines, for example, the difference in phenotypes led to dramatically different subcellular distribution and trafficking of 27 nm anionic quantum dots [41].

The experiments described herein characterize the uptake of 6 nm TiO_2 nanoparticles and TiO_2-ARS nanoconjugates in PC-3M cells. A quantitative flow cytometry approach, confocal microscopy, and ICP-MS were used to determine the cellular mechanisms and kinetics involved in TiO_2 nanoparticle internalization. In competition experiment in Figure 1.B. the morphology of the cell treated with competitor particles in addition to TiO_2-ARS was altered, with large vacuoles possibly filled with nanoparticles. However, the competitor TiO_2 nanoparticle concentration was 540 ng/ml of TiO_2 and in the absence of photoactivation anatase TiO2 nanoparticles are considered to become toxic only at 10 fold higher concentrations than the one used [39]. In Figure 4C, the data obtained for inhibition of Caveolin-Mediated Endocytosis by genistein showed only marginal significance. This result is most likely the outcome of the fact that Cav-Me is not a very prominent enocytosis mechanism in cells of PC-3 lineage [41-42] hence, the uptake that occurs in parallel and independent of Cav-Me overpowers the results of Cav-Me inhibition. In Figure 5B inhibition of the uptake following any of the three modes of inhibition shows a decrease but low significance values due to large variation between experiments. We expect that this may be caused by the fact that (at the time point investigated) no more than 50% of the cells take up the nanoparticles and the presence of many “empty” cells complicates interpretation of

the data, and most importantly the fact that whenever one mechanism of uptake is inhibited, two active uptake mechanism remain. When all three endocytic mechanisms were inhibited by low temperature exposure (Figure 5A), inhibition results obtained by ICP-MS showed high statistical significance.

Summarily, these studies revealed that nearly all of the nanoparticle (nanoconjugate)-cell uptake was metabolically dependent, and each one of the major endocytic mechanisms in PC-3M cells can be utilized for uptake of nanoconjugates. This can be explained in part by the fact that the nanoconjugates are smaller than any one of the vesicles formed during endocytosis. Clathrin-coated vesicles have a general diameter of nearly 120 nm; caveosomes range between 50 and 80 nm, while macropinosomes are the largest and most "leaky" with diameters from 500 to 2,000 nm [18]. Thus, it is possible for nanoconjugates to enter cells by any one of the possible endocytic mechanisms. While nanoparticle uptake was metabolically-dependent, it was non-specific in terms of a particular endocytic mechanism. In such a case, most prominent mechanism of uptake would be the one most prominent in the given cell type. In PC-3M cells two primary endocytic mechanisms are CME and macropinocytosis. [41-42] This matches well with the two most prominent processes of nanoparticle and nanoconjugate uptake detected through our work. Therefore, non-targeted uptake of nanoparticles by cells is highly feasible, which allows that the retention and intracellular trafficking of nanoconjugates become the mechanisms that ultimately dictate nanoconjugate quantity in cells.

Acknowledgments

This work was supported by NIH Grants: CA107467, EB002100, P50 CA89018, U54CA119341.

References

1. Paunesku T, Rajh T, Wiederrecht G, Maser J, Vogt S, Stojicevic N, et al. Biology of TiO2-oligonucleotide nanocomposites. Nat Mater. 2003; 2(5):343–6. [PubMed: 12692534]
2. Zhang AP, Sun YP. Photocatalytic killing effect of TiO2 nanoparticles on Ls-174-t human colon carcinoma cells. World J Gastroenterol. 2004; 10(21):3191–3. [PubMed: 15457572]
3. Blake DM, Maness PC, Huang Z, Wolfrum EJ, Huang J, Jacoby WA. Application of the Photocatalytic Chemistry of Titanium Dioxide to Disinfection and the Killing of Cancer Cells. Separation and Purification Methods. 1999; 28(1):1–50.
4. Sang X, Phan TG, Sugihara S, Yagyu F, Okitsu S, Maneekarn N, et al. Photocatalytic inactivation of diarrheal viruses by visible-light-catalytic titanium dioxide. Clin Lab. 2007; 53(7-8):413–21. [PubMed: 17821945]
5. Wu HP, Cheng TL, Tseng WL. Phosphate-modified TiO2 nanoparticles for selective detection of dopamine, levodopa, adrenaline, and catechol based on fluorescence quenching. Langmuir. 2007; 23(14):7880–5. [PubMed: 17564470]
6. Tsuang YH, Sun JS, Huang YC, Lu CH, Chang WH, Wang CC. Studies of photokilling of bacteria using titanium dioxide nanoparticles. Artif Organs. 2008; 32(2):167–74. [PubMed: 18269355]
7. Gogniat G, Thyssen M, Denis M, Pulgarin C, Dukan S. The bactericidal effect of TiO2 photocatalysis involves adsorption onto catalyst and the loss of membrane integrity. FEMS Microbiol Lett. 2006; 258(1):18–24. [PubMed: 16630249]
8. Cho M, Chung H, Choi W, Yoon J. Different inactivation behaviors of MS-2 phage and Escherichia coli in TiO2 photocatalytic disinfection. Appl Environ Microbiol. 2005; 71(1):270–5. [PubMed: 15640197]
9. Chen WJ, Tsai PJ, Chen YC. Functional Fe3O4/TiO2 core/shell magnetic nanoparticles as photokilling agents for pathogenic bacteria. Small. 2008; 4(4):485–91. [PubMed: 18348230]
10. Garabrant DH, Fine LJ, Oliver C, Bernstein L, Peters JM. Abnormalities of pulmonary function and pleural disease among titanium metal production workers. Scand J Work Environ Health. 1987; 13(1):47–51. [PubMed: 3495034]

11. Fayerweather WE, Karns ME, Gilby PG, Chen JL. Epidemiologic study of lung cancer mortality in workers exposed to titanium tetrachloride. J Occup Med. 1992; 34(2):164–9. [PubMed: 1597772]
12. Bernard BK, Osheroff MR, Hofmann A, Mennear JH. Toxicology and carcinogenesis studies of dietary titanium dioxide-coated mica in male and female Fischer 344 rats. J Toxicol Environ Health. 1990; 29(4):417–29. [PubMed: 2325155]
13. Bestak R, Halliday GM. Sunscreens protect from UV-promoted squamous cell carcinoma in mice chronically irradiated with doses of UV radiation insufficient to cause edema. Photochem Photobiol. 1996; 64(1):188–93. [PubMed: 8787013]
14. Maggos T, Bartzis JG, Liakou M, Gobin C. Photocatalytic degradation of NOx gases using TiO2-containing paint: a real scale study. J Hazard Mater. 2007; 146(3):668–73. [PubMed: 17532129]
15. Thurn KT, Paunesku T, Wu A, Brown EM, Lai B, Vogt S, et al. Labeling TiO2 nanoparticles with dyes for optical fluorescence microscopy and determination of TiO2-DNA nanoconjugate stability. Small. 2009; 5(11):1318–25. [PubMed: 19242946]
16. Rajh T, Chen LX, Lukas K, Liu T, Thurnauer MC, Tiede DM. Surface Restructuring of Nanoparticles: An Efficient Route for Ligand-Metal Oxide Crosstalk. J Phys Chem B. 2002; 106(41):10543–52.
17. Rajh T, Nedeljkovic JM, Chen LX, Poluektov O, Thurnauer MC. Improving Optical and Charge Separation Properties of Nanocrystalline TiO2 by Surface Modification with Vitamin C. J Phys Chem B. 1999; 103(18):3515–9.
18. Johannes L, Lamaze C. Clathrin-dependent or not: is it still the question? Traffic. 2002; 3(7):443–51. [PubMed: 12047552]
19. Kirkham M, Parton RG. Clathrin-independent endocytosis: new insights into caveolae and non-caveolar lipid raft carriers. Biochim Biophys Acta. 2005; 1746(3):349–63. [PubMed: 16440447]
20. Mosesson Y, Mills GB, Yarden Y. Derailed endocytosis: an emerging feature of cancer. Nat Rev Cancer. 2008; 8(11):835–50. [PubMed: 18948996]
21. Larkin JM, Brown MS, Goldstein JL, Anderson RG. Depletion of intracellular potassium arrests coated pit formation and receptor-mediated endocytosis in fibroblasts. Cell. 1983; 33(1):273–85. [PubMed: 6147196]
22. Harush-Frenkel O, Debotton N, Benita S, Altschuler Y. Targeting of nanoparticles to the clathrin-mediated endocytic pathway. Biochem Biophys Res Commun. 2007; 353(1):26–32. [PubMed: 17184736]
23. Aoki T, Nomura R, Fujimoto T. Tyrosine phosphorylation of caveolin-1 in the endothelium. Exp Cell Res. 1999; 253(2):629–36. [PubMed: 10585286]
24. Merrifield CJ. Seeing is believing: imaging actin dynamics at single sites of endocytosis. Trends Cell Biol. 2004; 14(7):352–8. [PubMed: 15246428]
25. Kaksonen M, Toret CP, Drubin DG. Harnessing actin dynamics for clathrin-mediated endocytosis. Nat Rev Mol Cell Biol. 2006; 7(6):404–14. [PubMed: 16723976]
26. Ivanov AI. Pharmacological inhibition of endocytic pathways: is it specific enough to be useful? Methods Mol Biol. 2008; 440:15–33. [PubMed: 18369934]
27. Lai SK, Hida K, Man ST, Chen C, Machamer C, Schroer TA, et al. Privileged delivery of polymer nanoparticles to the perinuclear region of live cells via a non-clathrin, non-degradative pathway. Biomaterials. 2007; 28(18):2876–84. [PubMed: 17363053]
28. Chung TH, Wu SH, Yao M, Lu CW, Lin YS, Hung Y, et al. The effect of surface charge on the uptake and biological function of mesoporous silica nanoparticles in 3T3-L1 cells and human mesenchymal stem cells. Biomaterials. 2007
29. Gratton SE, Ropp PA, Pohlhaus PD, Luft JC, Madden VJ, Napier ME, et al. The effect of particle design on cellular internalization pathways. Proc Natl Acad Sci U S A. 2008; 105(33):11613–8. [PubMed: 18697944]
30. Harush-Frenkel O, Rozentur E, Benita S, Altschuler Y. Surface charge of nanoparticles determines their endocytic and transcytotic pathway in polarized MDCK cells. Biomacromolecules. 2008; 9(2):435–43. [PubMed: 18189360]
31. Thurn K, Brown E, Wu A, Vogt S, Lai B, Maser J, et al. Nanoparticles for Applications in Cellular Imaging. Nanoscale Research Letters. 2007; 2(9):430.

32. Singh S, Shi T, Duffin R, Albrecht C, van Berlo D, Hohr D, et al. Endocytosis, oxidative stress and IL-8 expression in human lung epithelial cells upon treatment with fine and ultrafine TiO2: role of the specific surface area and of surface methylation of the particles. Toxicol Appl Pharmacol. 2007; 222(2):141–51. [PubMed: 17599375]
33. Wu A, Paunesku Tatjana, Brown Eric MB, Babbo Angela, Cruz Cecille, Aslam Mohamed, Dravid Vinayak, Woloschak Gayle E. Titanium Dioxide Nanoparticles Assembled by DNA Molecules Hybridization and Loading of DNA Interacting Proteins. NANO. 2008:27–36. [PubMed: 19890457]
34. Bergan R, K E, Nguyen P, Trepel J, Ingui C, Neckers L. Genistein-stimulated adherence of prostate cancer cells is associated with the binding of focal adhesion kinase to beta-1-integrin. Clin Exp Metastasis. 1996; 14:389–98. [PubMed: 8878413]
35. Altankov G, Grinnell F. Depletion of intracellular potassium disrupts coated pits and reversibly inhibits cell polarization during fibroblast spreading. J Cell Biol. 1993; 120(6):1449–59. [PubMed: 8449988]
36. Carpentier JL, Sawano F, Geiger D, Gorden P, Perrelet A, Orci L. Potassium depletion and hypertonic medium reduce “non-coated” and clathrin-coated pit formation, as well as endocytosis through these two gates. J Cell Physiol. 1989; 138(3):519–26. [PubMed: 2466853]
37. Hansen SH, Sandvig K, van Deurs B. Clathrin and HA2 adaptors: effects of potassium depletion, hypertonic medium, and cytosol acidification. J Cell Biol. 1993; 121(1):61–72. [PubMed: 8458873]
38. Singh RD, Puri V, Valiyaveettil JT, Marks DL, Bittman R, Pagano RE. Selective caveolin-1-dependent endocytosis of glycosphingolipids. Mol Biol Cell. 2003; 14(8):3254–65. [PubMed: 12925761]
39. Suh WH, Suslick KS, et al. Nanotechnology, nanotoxicology, and neuroscience. Progress in Neurobiology. 2009; 87(3):133–70. [PubMed: 18926873]
40. Lu Z, Ghosh S, Wang Z, Hunter T. Downregulation of caveolin-1 function by EGF leads to the loss of E-cadherin, increased transcriptional activity of beta-catenin, and enhanced tumor cell invasion. Cancer Cell. 2003; 4(6):499–515. [PubMed: 14706341]
41. Barua S, Rege K. Cancer-cell-phenotype-dependent differential intracellular trafficking of unconjugated quantum dots. Small. 2009; 5(3):370–6. [PubMed: 19089841]
42. Hill MM, B M, Luetterforst R, Kirkham M, Kirkham A, Nixon SJ, Walser P, Abankwa D, Oorschot VM, Martin S, Hancock JF, Parton RG. PTRF-Cavin, a conserved cytoplasmic protein required for caveola formation and function. Cell. 2008; 132(1):113–24. [PubMed: 18191225]

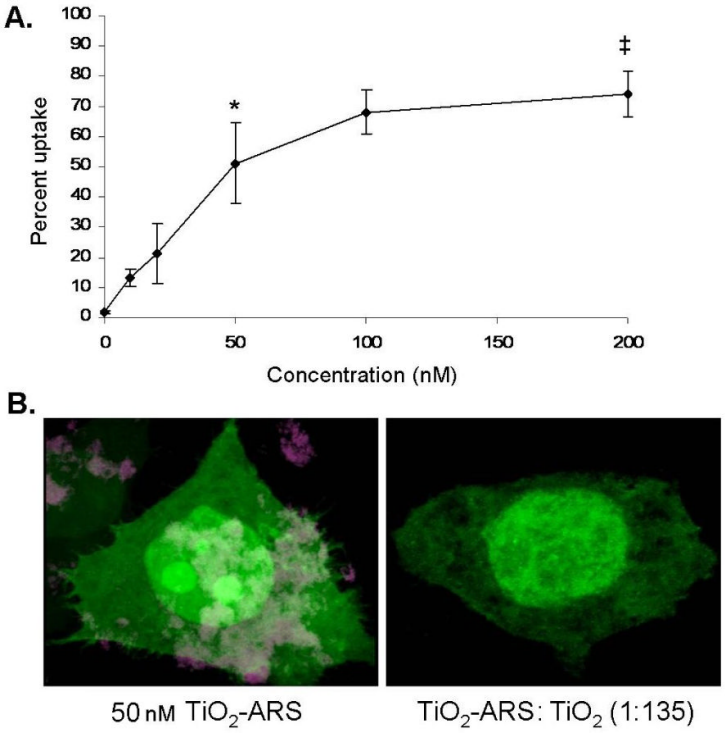

Figure 1.

Concentration and Competitor Dependent Uptake of TiO_2-ARS Nanoconjugates. **A.** Serum starved PC-3M cells were treated with a range of concentrations of fluorescently labeled nanoconjugates (0-200 nM). After one hour, the cells were washed to minimize surface bound nanoparticles, and analyzed by flow cytometry. There was a statistically significant increase in signal for cells treated with 50 nM nanoparticles (4 ng/ml) compared to lower nanoparticle concentrations (*$p<0.001$) (n=3). There was also a significant difference in uptake between cells treated with 50 and 200 nM (‡$p<0.05$). **B.** GFP expressing cells were treated with 50 nM of TiO_2-ARS nanoconjugates alone (left) or in combination with a 135 fold excess of unlabeled nanoparticles (6.7 μM) (right). Due to the significance of surface bound nanoparticles for this experiment, neither cell sample was glycine washed. Cells were fixed in 4% paraformaldehyde and imaged by laser scanning confocal microscopy. Cytoplasm and nucleus were both filled with GFP (green) while TiO_2-ARS nanoparticles(maroon) could be seen only in the absence of TiO_2 nanoparticle competition.

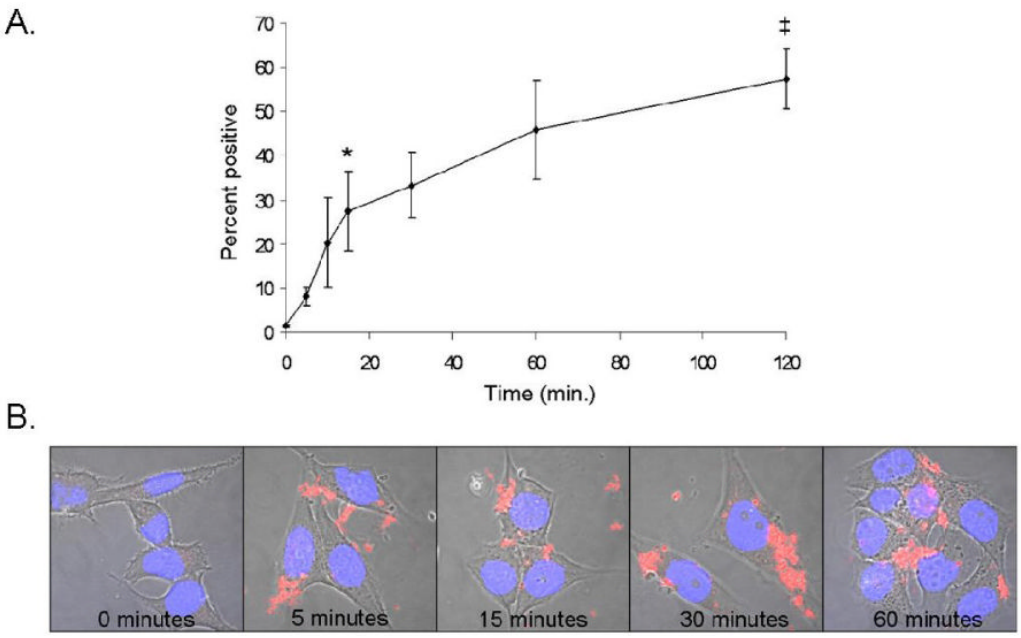

Figure 2.

Time-Dependent Uptake of TiO_2-ARS Nanoconjugates. **A.** PC-3M cells were treated with 50 nM of TiO_2-ARS for 0-120 minutes before analysis by flow cytometry. A statistically significant uptake was obtained by 15 minutes (*$p<0.05$), and the difference in uptake between cells treated for 15 and 120 minutes was statistically significant as well (‡$p<0.01$), but not the difference between cells treated for 60 and 120 minutes ($p>0.05$) (n=3). **B.** Confocal microscopy images of cells treated with 50 nM of TiO_2-ARS nanoconjugates (red) for the time points indicated. Blue (Hoechst dye) indicates position of the nucleus.

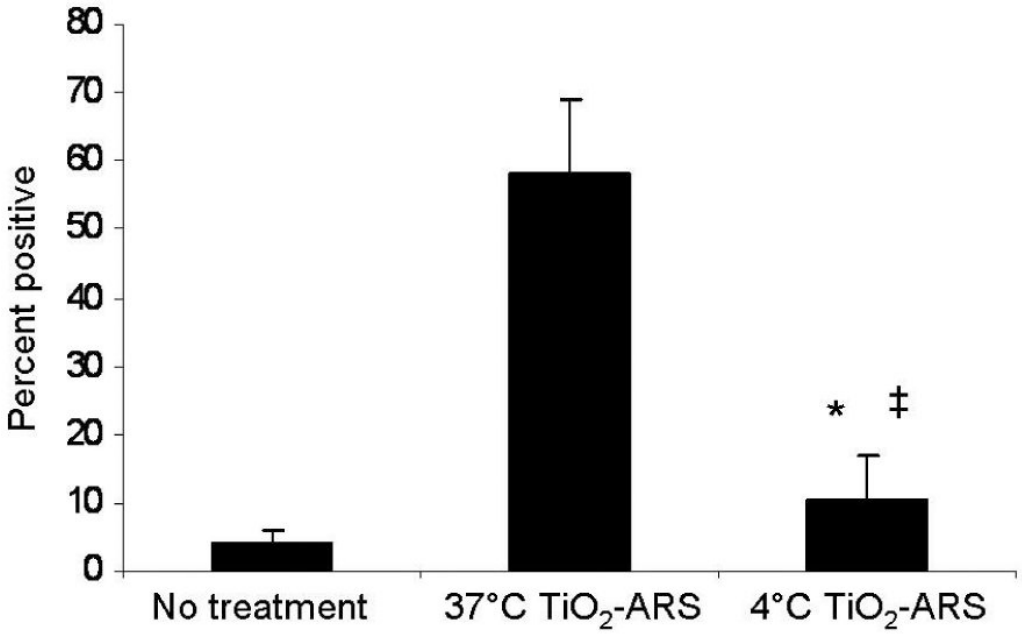

Figure 3.

Effect of Temperature on TiO_2-ARS Nanoconjugate Internalization. PC-3M cells were treated with 50 nM of fluorescent nanoconjugates (TiO_2-ARS) at 37°C or 4°C. Subsequent analysis by flow cytometry showed a significant decrease in fluorescence for cells treated at 4°C compared to 37°C (*$p<0.0001$). There was also a statistically significant difference in fluorescence between untreated cells and cells treated at the lower temperature (‡$p<0.05$) (n=6).

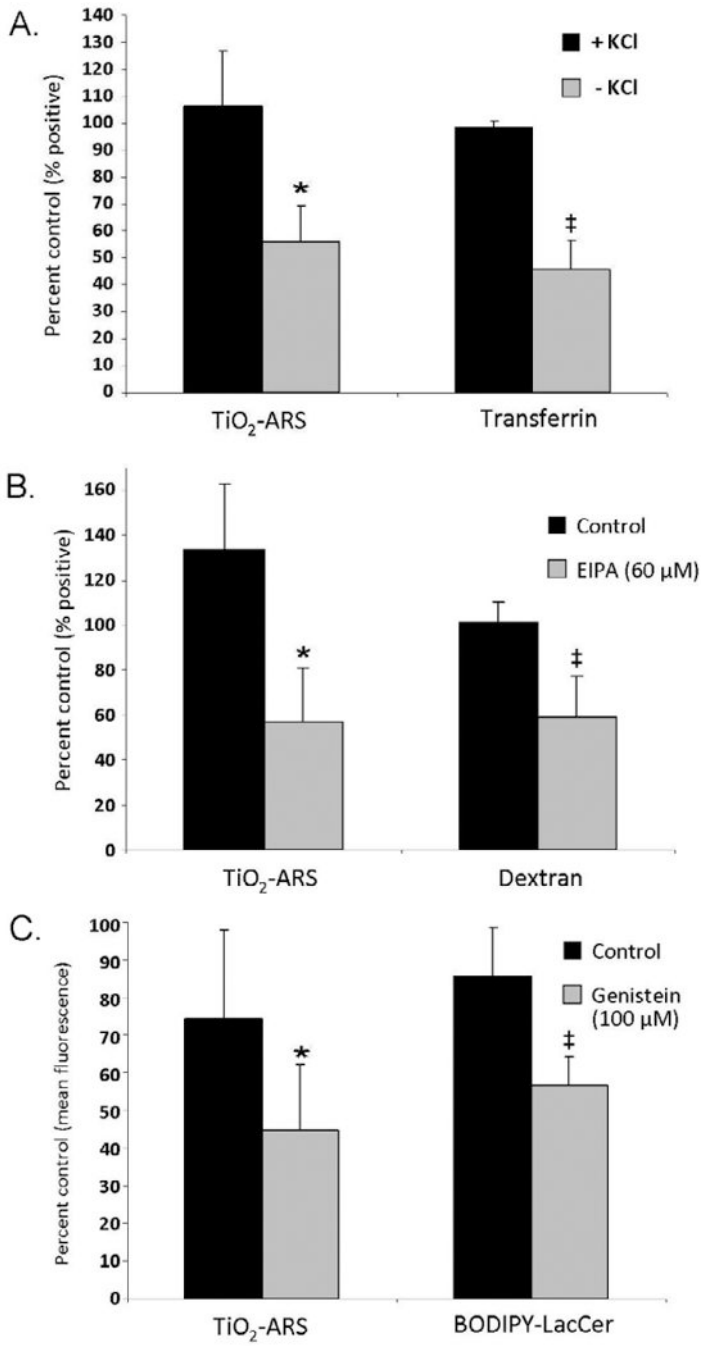

Figure 4.

Effect of Endocytosis Inhibitors on TiO_2-ARS Nanoconjugate Uptake. **A.** Potassium depletion modulates Clathrin Mediated Endocytosis (CME). Control cells were supplemented with 20 μM of potassium at all steps (+KCl). Fluorescent transferrin was used as a marker for CME. There was a statistically significant decrease in both TiO_2-ARS (*$p<0.05$) and transferrin (‡$p<0.05$) associated fluorescence in cells depleted of potassium ($n=3$). **B.** Role of Macropinocytosis in TiO_2-ARS endocytosiswas evaluated by using cells pre-treated with 60 μM of EIPA. Astatistically significant decrease in the uptake of TiO_2–ARS nanoconjugates and fluorescently labeled macropinocytosis marker dextran-Alexa647. Nanoconjugate uptake was diminished compared to control cells (*$p<0.05$) as well as

dextran endocytosis (‡$p<0.05$) (n=3). **C.** Caveolin-Mediated Endocytosis (Cav-Me) was down-regulated with 100 μM genistein. Fluorescence of TiO_2-ARS treated cells decreased (*$0.1<p<0.05$), as well as uptake of BODIPY-LacCer, a marker of Cav-Me uptake, (‡$p<0.05$).

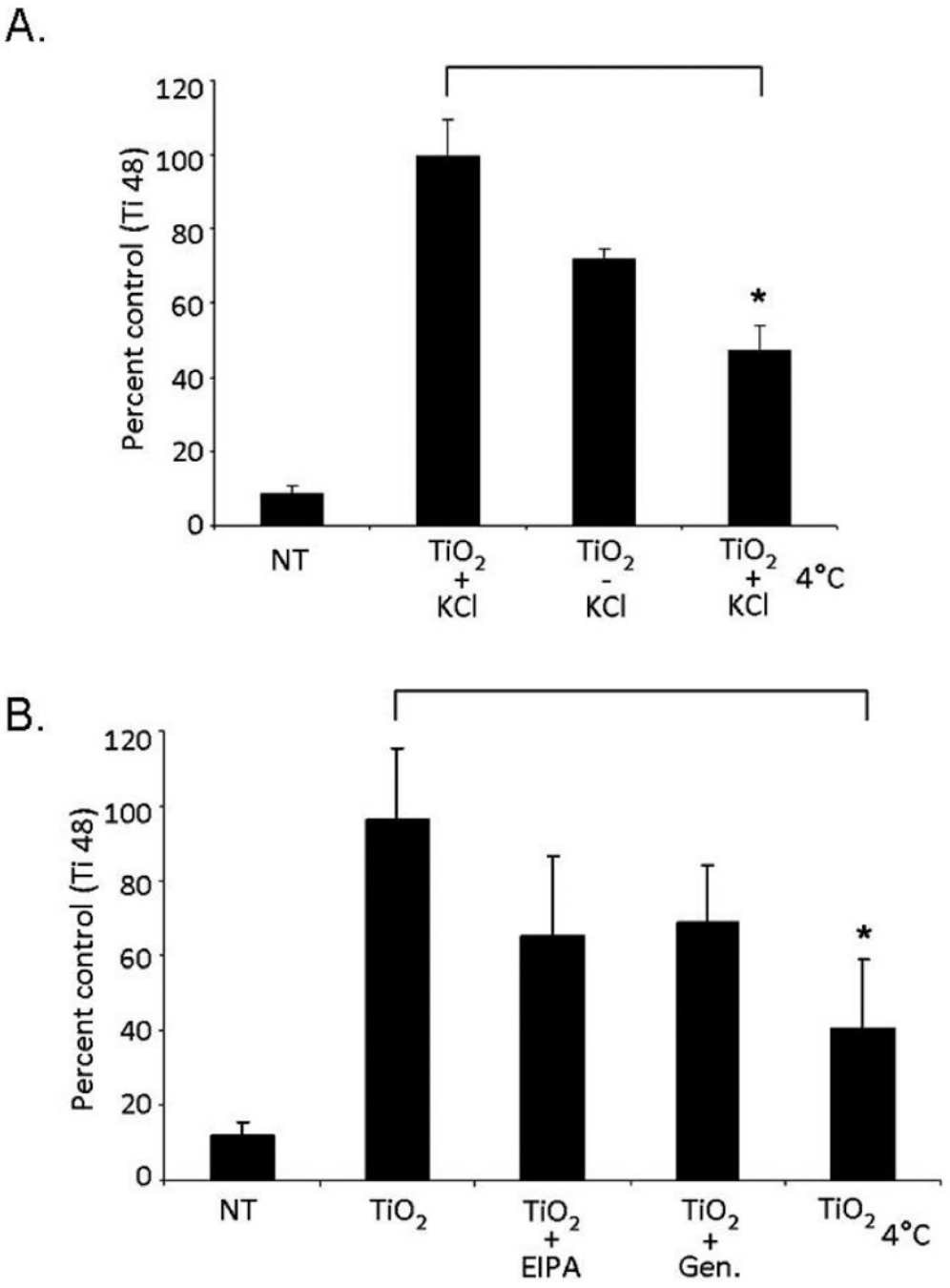

Figure 5.

Quantification of Cell Associated Titanium by ICP-MS. Cells were treated with TiO_2 nanoparticles after inhibition of specific endocytic pathways. **A.** Cell treatment in KCl-free medium. Control cells were supplemented with KCl at 37°C (TiO_2 + KCl) or treated at 4C (TiO_2 4°C) (*$p<0.05$) (n=3). **B.** Treatment with TiO_2 nanoparticles in serum free RPMI 1640 medium alone, with EIPA, genistein, or at low temperature. NT cells were nanoparticle free controls (*$p<0.05$) (n=3).